ACS APPLIED MATERIALS & INTERFACES

www.acsami.org

Research Article

In Situ Monitoring of Rolling Circle Amplification on a Solid Support by Surface Plasmon Resonance and Optical Waveguide Spectroscopy

Bernadette Lechner, Simone Hageneder, Katharina Schmidt, Mark P. Kreuzer, Rick Conzemius, Erik Reimhult, Ivan Barišić, and Jakub Dostalek*

Cite This: https://doi.org/10.1021/acsami.1c03715

Read Online

ACCESS | Metrics & More | Article Recommendations | Supporting Information

ABSTRACT: The growth of surface-attached single-stranded deoxyribonucleic acid (ssDNA) chains is monitored *in situ* using an evanescent wave optical biosensor that combines surface plasmon resonance (SPR) and optical waveguide spectroscopy (OWS). The "grafting-from" growth of ssDNA chains is facilitated by rolling circle amplification (RCA), and the gradual prolongation of ssDNA chains anchored to a gold sensor surface is optically tracked in time. At a sufficient density of the polymer chains, the ssDNA takes on a brush architecture with a thickness exceeding 10 μm, supporting a spectrum of guided optical waves traveling along the metallic sensor surface. The simultaneous probing of this interface with the confined optical field of surface plasmons and additional more delocalized dielectric optical waveguide modes enables accurate *in situ* measurement of the ssDNA brush thickness, polymer volume content, and density gradients. We report for the first time on the utilization of the SPR/OWS technique for the measurement of the RCA speed on a solid surface that can be compared to that in bulk solutions. In addition, the control of ssDNA brush properties by changing the grafting density and ionic strength and post-modification via affinity reaction with complementary short ssDNA staples is discussed. These observations may provide important leads for tailoring RCA toward sensitive and rapid assays in affinity-based biosensors.

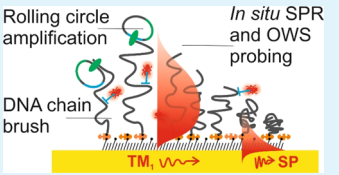

KEYWORDS: *rolling circle amplification, DNA, polyelectrolyte brushes, surface plasmon resonance, optical waveguide spectroscopy, surface plasmon-enhanced fluorescence, biointerfaces*

INTRODUCTION

The analysis of nucleic acids using polymerase chain reaction (PCR) has become a central method in numerous important fields ranging from screening hereditary diseases, detecting infectious pathogens, and cancer diagnosis to forensics and food quality control.[1−5] In the past decades, PCR-based methods have been gradually advancing, and we witnessed their implementation in a broad spectrum of analytical tools, including real-time PCR, digital PCR, and DNA sequencing.[6−8] In addition, there are pursued alternative approaches to PCR that allow a faster and simpler analysis of nucleic acid-based analytes without the need of thermocycling, such as isothermal rolling circle amplification (RCA)[9−11] and loop-mediated isothermal amplification (LAMP).[12,13] All these methods rely on enzymatic reactions with nucleic acids and are predominantly used in bulk solutions. However, the deployment of DNA amplification reactions at solid surfaces holds the potential to expand the performance of DNA analytical technologies through, for example, efficient multiplexing.[14,15] In addition, surface DNA amplification reactions may open doors to other types of sensor modalities and assay amplification strategies suitable for the detection of different analytes, including proteins that cannot be directly amplified and are typically detected by immunoassays.[16−18]

RCA enables generating densely packed single-stranded deoxyribonucleic acid (ssDNA) chains that form polyelectrolyte brush layers. Common techniques to observe such surface-attached polymer chains are ellipsometry,[19,20] fluorescence imaging,[21,22] X-ray photoelectron spectroscopy,[23] and angle-resolved near-edge X-ray absorption fine structure spectroscopy (NEXAFS).[24] However, these techniques typically provide information on the final structure and cannot be used to monitor the RCA growth process. The observation of soft ssDNA brushes in contact with a solvent was performed by atomic force spectroscopy, and the obtained thickness was substantially lower compared to the length of the ssDNA chains.[25] A chain length of up to several kilobases was determined for RCA-grown ssDNA brushes using enzymatic cleavage from the surface and subsequent gel electrophoresis, yielding a prolongation rate in the order of magnitude of several tens of bases/sec at the surface.[25] It should be noted

Received: March 3, 2021
Accepted: June 16, 2021

Table 1. Overview of the Used Oligonucleotides and Their Respective Molecular Weight (M_w)[a]

Oligonucleotide	Sequence (5'→ 3')	M_w (kDa)
Linear padlock probe (LP) (TS+/.../C2CA+/.../TS+)	TGTGATACAGCTTTCTTGCGCGTGTATGCAGCTCCTCGAGTAGCCGC AGTTCGCGCCGCAGGGCCGATACGTGTAACTTAT	25
Target (biotin/TS-)	biotin/TTTTTTTTTTTTTTTTTTTTAAGAAAGCTGTATCACAATAAGTT ACACGTATCGG	17.3
Labeling sequence (C2CA+/Cy5)	Cy5/GTGTATGCAGCTCCTCGAGTA	7
Randomized labeling sequence (random/Cy5)	Cy5/CAGCATCAGCTACGACTACGACTG	7.8
Stapling sequence (BA+/Cy5)	Cy5/TTATTGTGATACAGCTGGCCGATACGTGTAAC	10.4

[a]The (+) sequences are complementary to their corresponding (−) sequences, and colors indicate the parts that affinity hybridize.

that the growth of ssDNA using RCA on solid surfaces differs from that in bulk due to steric hindrance and slowed down diffusion of molecules associated with the interface carrying densely packed neighboring chains.[26]

Surface plasmon resonance (SPR) represents an established method for the observation of polymer thin films and molecular interaction analysis at solid surfaces.[27] It relies on the probing of (typically) a gold sensor surface using a tightly confined field of surface plasmons (SPs)—optical waves originating from the coupled collective oscillations of charge density and the respective electromagnetic field. SPR biosensors allow tracking molecular binding events accompanied by an increase or a re-distribution of the refractive index occurring in close proximity to the metallic sensor surface in real time.[28] To observe thicker polymer architectures such as crosslinked networks forming hydrogels, the SPR technique was combined with optical waveguide spectroscopy (OWS).[29,30] The analysis of detuning the resonant optical coupling to multiple dielectric waveguide modes (traveling along the surface with a more delocalized field profile than SPs) enables obtaining a more detailed picture of the interface. It allows for encoding multiple resonances to the measured optical spectra and, for example, accessing the information on the swelling and collapsing of polymer brushes in simpler means than with probing only by SPR.[31] Among others, OWS was utilized for the observation of hydrogel thin-film density gradients and for determining the responsive characteristics of polymers to external stimuli.[32,33] Moreover, the enhanced field intensity occurring upon the resonant excitation of SPs and optical waveguide (OW) modes has also been exploited for the optical amplification of weak fluorescence signals in a technique referred to as SP-enhanced fluorescence spectroscopy (SPFS).[34,35] The combined SPR and SPFS measurement allows distinguishing binding events of different molecular species and determining, for example, the incorporation of nucleotides to ssDNA strands attached to a gold surface using the Klenow fragment of a polymerase enzyme.[36]

We report on the combination of SPR, OWS, and SPFS for the *in situ* observation of RCA on a solid metal surface. This approach provided means for real-time monitoring of the growth of ssDNA chains that form a polyelectrolyte brush architecture with a thickness of above 10 μm. Furthermore, it was utilized to determine its important characteristics such as the grafting density of oligonucleotide chains, polymer volume content, time-dependent average chain length, reaction speed in terms of the number of nucleotides incorporated per minute, and the impact of the ionic strength on the thickness of the polyelectrolyte brush. Moreover, this technique was utilized for kinetic measurements of affinity binding of biomolecules occurring inside these brushes by labeling the chains and investigating the effect of intra- and inter-chain crosslinking with short ssDNA staples.

EXPERIMENTAL SECTION

Materials. The hydroxyl-(HS-$[CH_2]_{11}$-EG_6-OH)- and biotin-(HS-$[CH_2]_{11}$-EG_6-biotin)-terminated alkane oligo(ethylene glycol) (OEG)-thiols were purchased from ProChimia Surfaces (Poland). Phosphate-buffered saline (PBS, 137 mM NaCl, 2.7 mM KCl, 12 mM phosphate, pH = 7.4), nuclease-free water (NFW), Tween 20, and ethanol (EtOH) were obtained from VWR Chemicals (Germany). PBS Tween (PBST) was prepared by adding Tween 20 [0.05% (v/v)] to PBS. Hellmanex III, sodium chloride (NaCl), calcium chloride ($CaCl_2$), potassium chloride (KCl), magnesium chloride ($MgCl_2$), and sucrose were ordered from Sigma-Aldrich (Germany). Bovine serum albumin (BSA) was purchased from New England Biolabs (United Kingdom) and was diluted with NFW to a final concentration of 0.2 mg/mL (NFW-BSA). Neutravidin (NA, M_w = 67 kDa), phi29 DNA polymerase (φ-29 Pol), and deoxynucleotide triphosphates (dNTPs) were obtained from Thermo Scientific (Germany) and Ampligase DNA ligase from Biozym (Germany). The DNA oligonucleotides, summarized in Table 1, were acquired from Integrated DNA Technologies (Belgium).

Sensor Chip Preparation. Substrates made from BK7 (Assistant, Germany) or N-LASF9 (Hellma GmbH, Germany) glass were subsequently sonicated in 1% (v/v) Hellmanex III, ultrapure water ($R \geq 18.2$ MΩ/cm^2), and ethanol, followed by thorough rinsing with pure ethanol and drying in a stream of pressured air. Afterward, they were loaded into a vacuum thermal evaporator (HHV Ltd, Auto306 Lab Coater, UK) to deposit 2 nm-thick chromium and 50 nm-thick gold (MaTeck, Germany) layers in a vacuum better than 10^{-6} mbar. The freshly prepared gold layers were modified using a mixed-thiol self-assembled monolayer (SAM) by immersion in 1 mM ethanolic solution containing a mixture of thiols with biotin and hydroxyl headgroups dissolved at a molar ratio of 1:4. After overnight incubation, the glass substrates with a SAM-modified gold surface were rinsed with pure EtOH, dried under a nitrogen stream, and stored in the dark under an argon atmosphere until further use.

Growth of the ssDNA Brushes. NA (125 μg/mL in PBST) was flowed over the sensor surface for 90 min and allowed to bind to the biotin-functionalized SPR sensor chip, which was modified with a mixed-thiol SAM. The surface was rinsed with PBST, and the biotinylated target sequence (biotin/TS) hybridized with the circular padlock (CP) probe was reacted with the sensor surface for 30 min. Then, RCA was conducted for 1−4 h under a continuous flow of a solution with phi29-DNA polymerase (φ29-Pol) and the respective reagents. A detailed description of the preparation of the CP and the RCA reaction on the surface can be found below.

Ligation. The padlock probe sequence (LP, 90 nM) was ligated in the presence of the biotinylated target sequence (biotin/TS-, 40 nM) and 75 units of DNA ligase in NFW-BSA with the respective ligation

https://doi.org/10.1021/acsami.1c03715
ACS Appl. Mater. Interfaces XXXX, XXX, XXX−XXX

buffer (20 mM Tris-HCl, 25 mM KCl, 10 mM $MgCl_2$, 0.5 mM NAD, and 0.01% Triton X-100) in a total volume of 500 μL. Ligation was conducted for 2 h at 50 °C at 700 rpm on a shaker, and it was terminated by heating the solution to 85 °C for 5 min.

Rolling Circle Amplification. RCA was conducted with 100 units of φ29-Pol and 100 μM of each dNTP in NFW-BSA with the respective buffer constituents (33 mM Tris-acetate, 10 mM Mg-acetate, 66 mM K-acetate, 0.1% Tween 20, and 1 mM DTT) in a total volume of 500 μL. Prior to the RCA, the sensor chip was rinsed with φ29-Pol buffer without the dNTPs to establish a baseline in the sensor response. The RCA product was hybridized with Cy5 fluorophore-labeled C2CA+ oligonucleotide (C2CA+/Cy5) at a concentration of 10 nM in PBST for 15 min, which was followed by a buffer-rinsing step for 5 min.

Optical Instrument. A home-built SPR/OWS optical system based on the Kretschmann configuration (see Figure 1) was used for

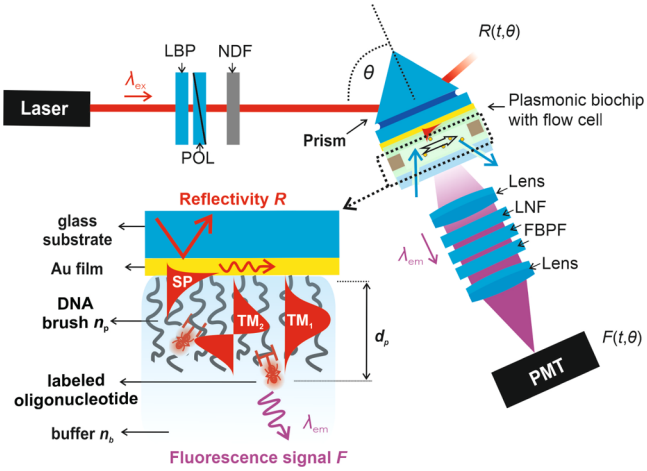

Figure 1. Optical configuration used for the combined SPR, OWS, and SPFS measurements.

the resonant excitation of SP and dielectric OW modes at the sensor chip carrying a gold layer with the mixed-thiol-OEG-OH/biotin SAM and in the course of the experiment generated ssDNA brushes. This sensor chip was optically matched to a 90° LASF9 glass prism base using refractive index immersion oil (Cargille Laboratories, USA) and was mounted on a rotation stage. A HeNe laser beam at a wavelength of λ_{ex} = 632.8 nm passed through a laser band-pass filter (LBF) and neutral density filter (NDF) and was coupled to the prism impinging at the sensor chip surface at a controlled angle of incidence θ. The intensity of the reflected beam R was measured with a photodiode connected to a lock-in amplifier. A transparent flow cell was clamped against the sensor chip to transport liquid samples along the sensor surface. The flow cell was composed of a glass substrate with drilled inlet and outlet ports and a thin PDMS gasket that defined a reaction chamber volume of 10 μL. The flow cell was connected with Tygon tubing (inner diameter = 0.25 mm) to a peristaltic pump to flow liquid samples kept at room temperature with a flow rate set to 50 μL/min. All reaction mixtures containing proteins and enzymes were continuously re-introduced by closing the tubing loop. The reflected beam intensity R was monitored as a function of the angle of incidence θ or time t to resolve changes in resonant excitation of SP and OW modes that manifest themselves as a series of dips in $R(\theta)$. The polarization of the excitation beam was set to transverse magnetic (TM) or transverse electric (TE) using a polarizer (POL). In addition, the resonantly coupled SPs and OWs were utilized for the excitation of Cy5 fluorophore labels conjugated with ssDNA that binds to the RCA-synthesized ssDNA chains at the sensor surface. These fluorophores emitted fluorescence light at a shifted wavelength of λ_{em} = 670 nm, which was collected through the transparent flow cell using a lens and made to pass through a fluorescence band-pass filter (FBPF, 670FS10-25 from Andover Corporation Optical Filter, USA) and a laser notch (LNF, XNF-632.8-25.0M, CVI Melles Griot, USA) filter. The spectrally clean fluorescence beam was focused using an additional lens at the input of a photomultiplier tube (PMT, H6240-01 from Hamamatsu Photonics, Japan). The intensity of the fluorescence signal F was measured with a photon counter (53131A from Agilent, USA) in counts per second (cps). The optical instrument was operated with dedicated software (Wasplas, developed at Max Planck Institute for Polymer Research, Mainz, Germany; see more details in the Supporting Information).

Sensor Readout and Data Analysis. The SPR measurement started with recording the angular reflectivity spectrum $R(\theta)$ for a gold sensor surface that carried a mixed-thiol SAM in contact with PBST. Time-dependent measurements $R(t)$ were performed at an angle of incidence θ set in the vicinity to the SPR dip within the range, where the reflectivity linearly decreases with the angle of incidence θ. The recorded variations in reflectivity $R(t)$ were converted to refractive index unit (RIU) changes using a calibration. This calibration was performed by measuring $R(t)$ upon the flow of aqueous solutions containing 1, 2, and 4% (w/w) of sucrose, which increases the bulk refractive index by $\Delta n_b = 1.4 \times 10^{-3}$, 2.9×10^{-3}, and 5.8×10^{-3} RIU, respectively. After each immobilization or reaction step (NA, target sequence|circular padlock, RCA), the sensor surface was rinsed with PBST, and an angular reflectivity spectrum $R(\theta)$ was recorded. These curves were fitted with a Fresnel reflectivity-based model using dedicated software (Winspall, developed at Max Planck Institute for Polymer Research, Mainz, Germany). The polymer brushes were approximated as a dielectric layer with a thickness d_p and refractive index n_p, which were determined by fitting the resonant angles of a series of dips in the measured reflectivity curves $R(\theta)$ that are associated with the resonant excitation of SP and OW modes. The modes measured in TE and TM polarization were fitted in parallel, and the birefringence was omitted.

The surface mass density of the polymer layer was calculated as $\Gamma = d_p(n_p - n_b)/(dn/dc)$, where n_p and n_b are the refractive indices of the attached layer and of the buffer, respectively, and d_p is the thickness of the protein/ssDNA layer. The incremental change in the refractive index with the concentration (dn/dc) for DNA and protein was set to 0.17 and 0.2 mm^3/mg, respectively.[37,38] Surface mass density Γ was obtained in ng/mm^2, and it was converted into a grafting density σ of attached molecules per area (in $nmol/mm^2$) using their respective molecular weights (M_w). A summary of the used mathematical models can be found in the Supporting Information.

RESULTS AND DISCUSSION

As illustrated in Figure 2, the "grafting-from" growth of ssDNA polymer chains was initiated by capturing a circular padlock (CP) probe that was hybridized with the target sequence (TS) to facilitate solid-phase RCA at the sensor surface.[39] The padlock probe sequence was designed to hybridize with the specific TS that is present in the clinically highly important antibiotic resistance gene bla_{OXA-48}.[40] For the proof of concept, the linear padlock probe (LP) was hybridized with the synthetic TS that was conjugated with biotin (biotin/TS-). The subsequent ligation reaction enzymatically sealed the gap between the 5′ and 3′ ends of the target recognition arms of the LP when hybridized with the TS. This step is highly specific and led to the circularization of the padlock probe—CP. Afterward, the created target sequence|circular padlock duplex (biotin/TS-|CP) was anchored to the sensor chip gold surface in an oriented manner.[41] This was done through biotin moieties incorporated to the mixed-thiol SAM, which allowed the binding of NA, serving as a linker for the immobilization of the biotin/TS-|CP construct.

Isothermal RCA was initiated by the addition of φ29-polymerase, which sequentially incorporates nucleotides (dNTPs) on the TS- free 3′ end to form long ssDNA chains composed of multiple reverse-complementary repeats of the

https://doi.org/10.1021/acsami.1c03715
ACS Appl. Mater. Interfaces XXXX, XXX, XXX−XXX

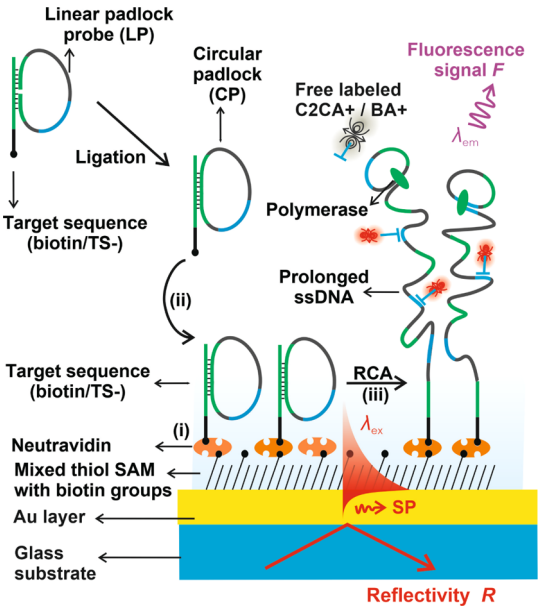

Figure 2. Schematics of the biointerface architecture and the growth of the ssDNA brush.

CP sequence. Then, the RCA product was reacted with C2CA + or BA+ oligonucleotides conjugated with Cy5 fluorophores (C2CA+/Cy5 and BA+/Cy5, respectively). All immobilization procedures were monitored using an optical setup, which combined surface plasmon resoance (SPR) and surface plasmon-enhanced fluorescence spectroscopy (SPFS) (see Figure 1). The SPR detection principle allowed us to acquire time-dependent kinetics of the sensor response $R(t)$, while the recorded angular reflectivity curves $R(\theta)$ were used for probing the biointerface with multiple SP and OW modes in order to determine changes in the ssDNA polymer architecture thickness d_p and refractive index n_p, reflecting increasing surface mass density Γ. Furthermore, the fluorescence intensity, originating from fluorophore-labeled biomolecules that were affinity-bound to the ssDNA chains and excited via the resonantly coupled SP and OW modes, was recorded in time $F(t)$ and as a function of the angle of incidence $F(\theta)$. These SPFS recordings enabled monitoring events that yield only subtle changes in the refractive index and hence cannot be measured with SPR.

Implementation of the Assay on a Plasmonic Sensor.

Figure 3a shows a typical SPR sensorgram $R(t)$ upon the subsequent binding of (i) NA, (ii) the biotin/TS oligonucleotide hybridized to the circular padlock probe—CP, and (iii) RCA followed by the binding of C2CA+/Cy5. The affinity binding of the tetravalent NA to the biotin headgroups on the thiol-SAM led to an increase in the SPR response to ΔR_{NA} = 3.8 mRIU. The free biotin-binding pockets allowed us to anchor the oligonucleotide biotin/TS|CP duplex in a following step, which changed the SPR response of $\Delta R_{biotin/TS|CP}$ = 1.2 mRIU. After the contacting of φ29-Pol and dNTPs with the sensor surface, a gradual increase in the sensor signal $R(t)$ was observed, which corresponds to the binding of the polymerase and the subsequent prolongation of ssDNA chains tethered to the sensor surface via the biotin tag. In this experiment, the RCA reaction was terminated after 1 h by removing nucleotides from the flow cell (through rinsing with a buffer), and an increase in the SPR signal ΔR_{RCA} = 2.3 mRIU was measured with respect to the baseline after the oligonucleotide immobilization. The abrupt jumps in the SPR response occurring upon rinsing the sensor surface with ligation and RCA buffers are ascribed to variations in the bulk refractive index n_b due to different buffer compositions. The generated ssDNA chains are composed of repeating C2CA—sequences and TS—sequences complementary to the CP. In order to confirm their presence, complementary C2CA+/Cy5 and control non-complementary (random/Cy5) Cy5-labeled oligonucleotides were reacted with the sensor surface after each reaction step. As seen in the recorded fluorescence signal $F(t)$ before conducting RCA, the signal increased abruptly after the injection of fluorophores conjugated to short oligonucleotides but dropped back to its baseline level after the rinsing with buffer. This rapid increase in the fluorescence signal is explained by the excitation of the Cy5 fluorophores in the bulk solution. After running the RCA, the introduction of the control non-complementary oligonucleotides conjugated with Cy5 showed a small change in the fluorescence intensity of $\Delta F_{random/Cy5}$ = 600 cps. However, the reaction with a specific oligonucleotide was accompanied by a 130-fold stronger increase in the fluorescence intensity of $\Delta F_{C2CA+/Cy5}$ = 80,000 cps, proving the successful synthesis of ssDNA chains by RCA.

To determine the surface mass density Γ of the incorporated molecules on the surface, the reflectivity curves $R(\theta)$ were measured in between each reaction step, as shown in Figure

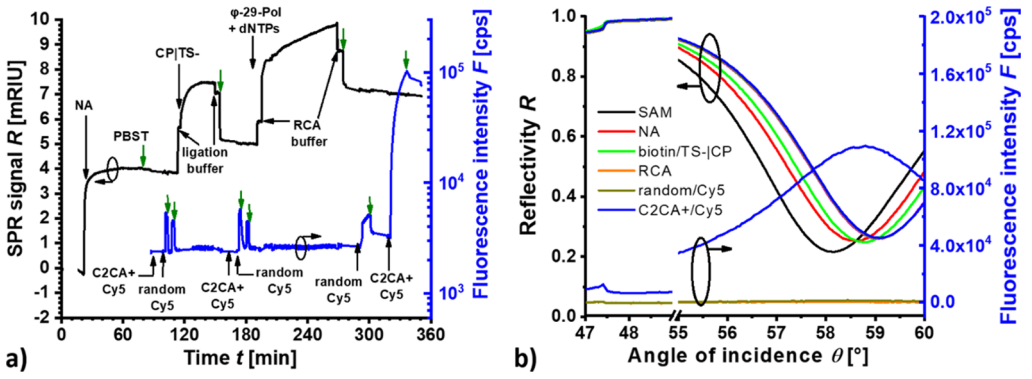

Figure 3. (a) Example of the kinetic SPR signal $R(t)$ and fluorescence signal $F(t)$ upon capture of neutravidin, the CP and the generation of the ssDNA polymer brush through RCA on the sensor surface. (b) Respective angular reflectivity $R(\theta)$ and fluorescence $F(\theta)$ scans measured between the reaction steps.

https://doi.org/10.1021/acsami.1c03715
ACS Appl. Mater. Interfaces XXXX, XXX, XXX−XXX

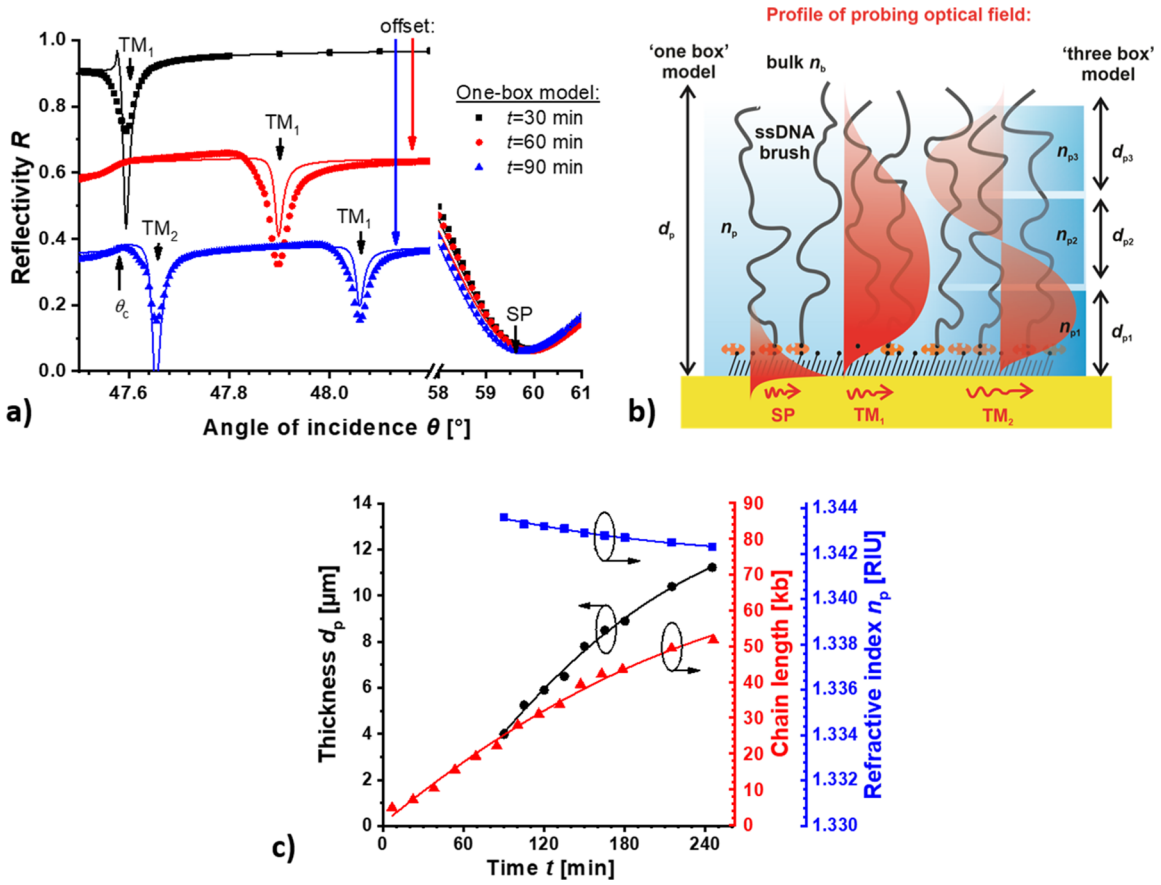

Figure 4. (a) Angular reflectivity curves $R(\theta)$ (measured data are shown as symbols, and fitted curves using the "one-box model" are showed as lines). For better data visualization, the reflectivity curves $R(\theta)$ measured at 60 and 90 min for $\theta < 50°$ are offset by a factor of 0.3 and 0.6, respectively (offset indicated with red and blue arrows). (b) Schematics of probing the ssDNA brushes with distinct distribution of electromagnetic field amplitude of SP and OW modes and used models approximating the optical properties of the brush. (c) Determined time-dependent thickness d_p and refractive index n_p together with estimated polymer chain length. Determined values are shown as symbols and fitted with a polynomial function (lines).

3b, and fitted with a Fresnel reflectivity-based model. The black curve in Figure 3b shows the resonant excitation of SPs on the gold surface carrying a mixed thiol SAM, which manifests itself as a dip in the angular reflectivity $R(\theta)$. This dip is centered at the resonance angle $\theta = 58.15°$, and it shifted to a higher angle ($\theta = 58.6°$) upon the conjugation of NA to the biotin headgroups and after immobilization of the biotin/TS|CP duplex ($\theta = 58.75°$). These shifts translate to a grafting density σ of 3.1×10^{-5} and 1.8×10^{-5} nmol/mm^2 for the immobilized NA and target|padlock duplex, respectively. A closer look at this number revealed that only ~59% of the immobilized NA molecules reacted with a biotin-tagged oligonucleotide strand. This can be ascribed to the fact that NA shows ~7 nm center-to-center distance at full surface coverage,[42] and thus, the subsequent reaction with the 81 nt circularized padlock probe exhibiting a diameter of ~9 nm was likely to be sterically hindered.[43]

The shift in the SPR angle after the RCA to $\theta = 59°$ cannot be independently attributed to the bound polymerase and the generated RCA product. However, the excitation of Cy5 fluorophores in $F(\theta)$ was only observed after hybridizing the RCA product with its specific C2CA+/Cy5 oligonucleotide. This proves the presence of the ssDNA chains within the evanescent field of SPs, as their excitation enhanced the emitted fluorescence intensity. Thus, it can be observed as a peak in the spectrum $F(\theta)$ at the angle where a dip occurs in the SPR reflectivity curve $R(\theta)$. It is worth noting that only the fluorescence-based measurement provides this confirmation, as the change in the SPR detection channel gave a negligible shift in $R(\theta)$ after the specific binding of C2CA+/Cy5 that exhibits too low molecular weight M_w.

***In Situ* Monitoring of Chain Growth.** Several research groups investigated RCA on the solid surface using SPR and reported that the measured output signal saturated, and increasing the reaction time was assumed to not change the properties of the generated ssDNA chains for reaction times, t, above 1 h.[44−48] In general, this optical measurement allows us to monitor changes occurring only within the evanescent field of SPs that probe a distance of up to about 100 nm from the gold surface. In the following study, we attempted to optically probe farther from the surface and investigate ssDNA chains generated by the RCA for several hours on the gold surface with a grafting density of CP probes $\sigma_{\text{biotin/TS|CP}} = 2.6 \times 10^{-5}$ nmol/mm^2 (detailed calculations can be found in the Supporting Information). In these measurements, we continuously recorded reflectivity curves $R(\theta)$ in order to *in situ* optically track the prolongation of ssDNA brushes every 15 min. Interestingly, after 30 min of reaction, we observed an additional resonant dip in $R(\theta)$ close to the critical angle $\theta_c = 47.5°$ (besides the SPR dip at $\theta \sim 59°$); see Figure 4a. This resonant dip in the reflectivity spectrum can be attributed to the resonant excitation of dielectric OW modes traveling along

https://doi.org/10.1021/acsami.1c03715
ACS Appl. Mater. Interfaces XXXX, XXX, XXX−XXX

the surface. The excitation of such waves (for transverse polarized light marked as $TM_{1,2,3...}$) is a signature of the presence of a ssDNA polymer layer with a refractive index n_p higher than that of the bulk solution n_b and a thickness d_p exceeding 100 nm. Furthermore, we took advantage of the interrogation of the resonant excitation of OW modes to optically probe DNA polymer strands stretching beyond the regular probing depth of SPR upon their prolongation by the RCA reaction (see Figure 4b). At thicknesses d_p > 100 nm, the growth of ssDNA chains occurs outside the evanescent field of SPs, and thus, only OWS enables their monitoring from the independent measurements of the thickness d_p and the refractive index n_p of the respective polymer layer. This was possible by fitting the measured angular reflectivity curves $R(\theta)$ exhibiting a series of resonant dips (Figure 4b) with a Fresnel reflectivity-based model. For the analysis of the obtained data, the surface-attached ssDNA brush was first represented by a homogeneous dielectric layer with a uniform refractive index n_p in contact with a semi-infinite medium exhibiting a bulk refractive index of the buffer (n_b = 1.336). This approach is referred to as the "one-box model," and Figure 4c shows the obtained time dependence of these two parameters, which reveals gradual incorporation of nucleotides by RCA that leads to the generation of d_p = 11.2 μm-thick brush after 4 h of reaction. In general, at least two resonant features need to be fitted to determine both the refractive index n_p and thickness d_p independently, and thus, this was possible only for times t > 90 min. Interestingly, the (average) refractive index n_p of the ssDNA brush determined from OWS was gradually decreasing upon the RCA reaction, reaching a value of n_p = 1.3423 after t = 240 min. This can indicate that the prolongation stops on some strands and the brush gets diluted as it grows away from the surface analogously to chain termination in a polymerization reaction (which is often observed for surface-initiated polymerization of thick polymer brushes). In the presented study, it would be the result of the loss of steric access to strands buried in the thick brush. Additionally, it can be seen that the SPR coupling angle gradually decreases in time after the initial phase of RCA. This occurs even at times t when the ssDNA chains grow far away from the SP evanescent field, and therefore, it can be explained by rearrangement of this part of the brush at close vicinity to the gold surface that is associated with possible chain stretching.

The respective gradually increasing thickness d_p and slowly decreasing refractive index n_p were used to calculate the accumulated surface mass density Γ_{RCA} at each given time point (see the Supporting Information for details). At the end of the reaction at time t = 4 h, a massive increase in the surface mass density of Γ_{RCA} = 415 ng/mm^2 was determined. This corresponds to ∼16 MDa ($\Gamma_{RCA}/\sigma_{biotin/TS|CP}$) or ∼52 kb per oligonucleotide strand and indicates that the padlock probe (81 nt) was in average amplified ∼640 times on each chain. Interestingly, the average (contour) length of the ssDNA chains obtained from the number of repeats of 48.6 nm-long LP yields about 31.2 μm. This value corresponds to the configuration, where the effective thickness of the brush d_p is almost a third of the contour length of the grafted ssDNA chains.

From the dependence of the number of nucleotides incorporated to the ssDNA polymer chains (shown as the red curve in Figure 4c), an average extension rate of ∼215 nt/min can be deduced. This value is substantially slower than the one obtained at 30 °C by Soengas et al. in bulk solutions yielding >10^3 nt/min.[49] At this point, it should be noted that the determined amplification rate should be seen as the minimum speed of nucleotide incorporation by φ 29-Pol on a solid support-based platform that is affected by the chain folding, gradual dilution when moving away from the surface, and diffusion of nucleotides to the surface.

As mentioned above, the chain prolongation does not proceed identically for all the chains, and a certain distribution of their length can be expected. In addition, the stretching of the chains can differ at the inner and outer sides of the brush. The impact of these phenomena can be assessed by determining the gradient of the ssDNA brush layer density in the direction perpendicular to the surface. As seen in Figure 5a, three or more OW modes ($TM_{1,2,3}$) became apparent in the measured reflectivity spectra $R(\theta)$ after 2 h of reaction, and then, a clear deviation between the measured and fitted curves occurs (we fitted the number of OW modes and the angular position of the first and last one). Therefore, the "one-box model" was extended by splitting the layer into three segments and fitting the refractive index independently for each of them. As schematically shown in Figure 4b, this refined model allows us to take into account a gradient in the brush density with a lower refractive index n_b of the layer on its outer interface (in contact with buffer) and a higher refractive index n_b at its inner surface (where it is attached to the gold surface). The fitting with such a "three-box model" is presented in Figure 5b for t =

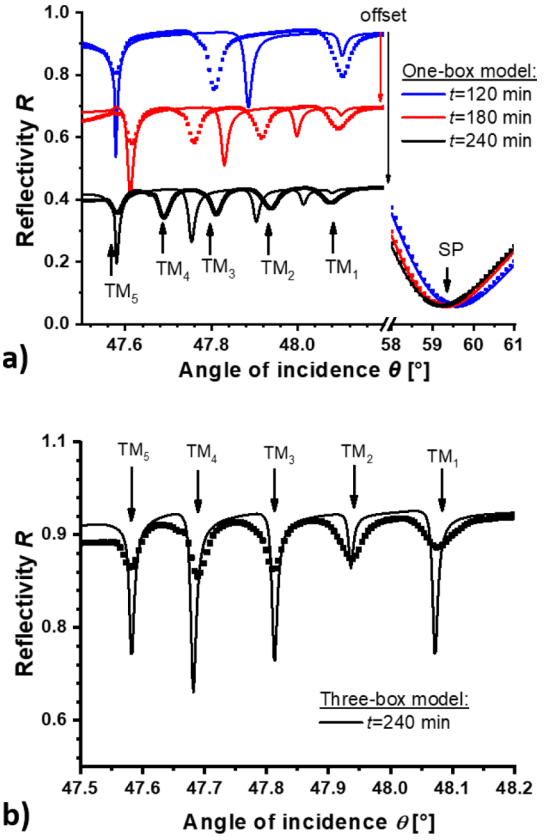

Figure 5. (a) Measured $R(\theta)$ at the growth time of t = 120, 180, and 245 min that is fitted with the Fresnel reflectivity model using the "one-box" approximation. The reflectivity curves $R(\theta)$ measured at 180 and 240 min are shifted, respectively, by a factor of 0.3 and 0.6 in respect to the one measured at 120 min. (b) Comparison of the fitting with "three-box" approximation for data acquired at t = 240 min.

https://doi.org/10.1021/acsami.1c03715
ACS Appl. Mater. Interfaces XXXX, XXX, XXX−XXX

240 min. It shows that the angular positions of all five supported OW modes can be fitted, and the first compartment exhibited a thickness of d_{p1} = 3.8 μm followed by the second one with d_{p2} = 6.0 and third with d_{p3} = 2.9 μm. The fitted refractive index decreased from n_{p1} = 1.3434 at the gold surface to n_{p2} = 1.3410 in the middle part and n_{p3} = 1.3384 for the outer segment of the polymer brush. This analysis suggests that the polymer volume content (proportional to the layer refractive index n_p) is decreasing with distance from the gold surface, and it can be ascribed to a length distribution of the RCA-generated ssDNA polymer chains or possibly more stretched conformation of polymer chains at the outer than the inner interface. The total thickness ($d_{p1} + d_{p2} + d_{p3}$ = 12.7 μm) is slightly higher than the one obtained in the "one-box model", and the weighted refractive index of the attached layer of $(n_{p1}\cdot d_{p1} + n_{p2}\cdot d_{p2} + n_{p3}\cdot d_{p3})/(d_{p1} + d_{p2} + d_{p3})$ = 1.3411 is slightly decreased. However, the corresponding overall surface mass density and respective average polymer chain length of 48 kb per immobilized padlock probe at a reaction duration of 240 min are comparable for both models.

Response of the ssDNA Brush to Ion Environments. Recent studies have shown that the DNA structure is highly dependent on its surrounding aqueous environment,[50] which is of high importance in sensor applications of surface-attached ssDNA brushes.[51] Especially, the presence of specific cation species causes changes in inter-nucleotide distances[52] and can strongly affect the grafting density[53,54] and hybridization regimes of DNA on solid supports.[55,56] Figure 6a shows a schematic of the effect of increasing ionic strength on the DNA brush, which leads to its compression or expansion. Furthermore, we exposed the ssDNA brush to electrolytes containing monovalent (NaCl and KCl) and divalent ($MgCl_2$ and $CaCl_2$) cations to study their impact on the ssDNA brush. The influence on DNA brush thickness d_p and its corresponding refractive index n_p was determined by fitting the reflectivity spectrum $R(\theta)$ and exhibiting SP and OW resonances with the "one-box model" approximation in different ionic solutions (we used ssDNA brushes prepared by RCA with a reaction time that did not allow for the probing with multiple OW modes, and thus, the more accurate "three-box model" was not possible to use). The refractive index of the bulk aqueous solution n_b was determined from SPR on a bare gold surface or from the position of the critical angle θ_c. An additional option for the observation of the swelling and collapsing of the ssDNA brushes offers the SP- and OW-enhanced fluorescence spectroscopy. After the affinity binding of Cy5-conjugated DNA strands (C2CA+/Cy5 or BA+/Cy5), such changes lead to variations in the fluorescence signal originating from the respective part of the architecture selectively probed with the SP or OW field. The evanescent field of resonantly excited SPs excites the fluorophores in a thin (~100 nm) slice at the inner side of the brush, whereas the OWs are more delocalized and can probe the whole brush volume (see Figure 4b). Therefore, compacting the ssDNA brush carrying affinity-bound molecules conjugated with fluorophores is associated with an increase in the SP-enhanced fluorescence signal, whereas the expansion of the structure has the opposite effect.

As the example in Figure 6b illustrates for the brush structures with C2CA+/Cy5, the exposure of the brush to an ionic solution can lead to the compression and expansion of the structure. The compression is manifested as a shift of the SPR to higher angles and the respective increase in the SP-

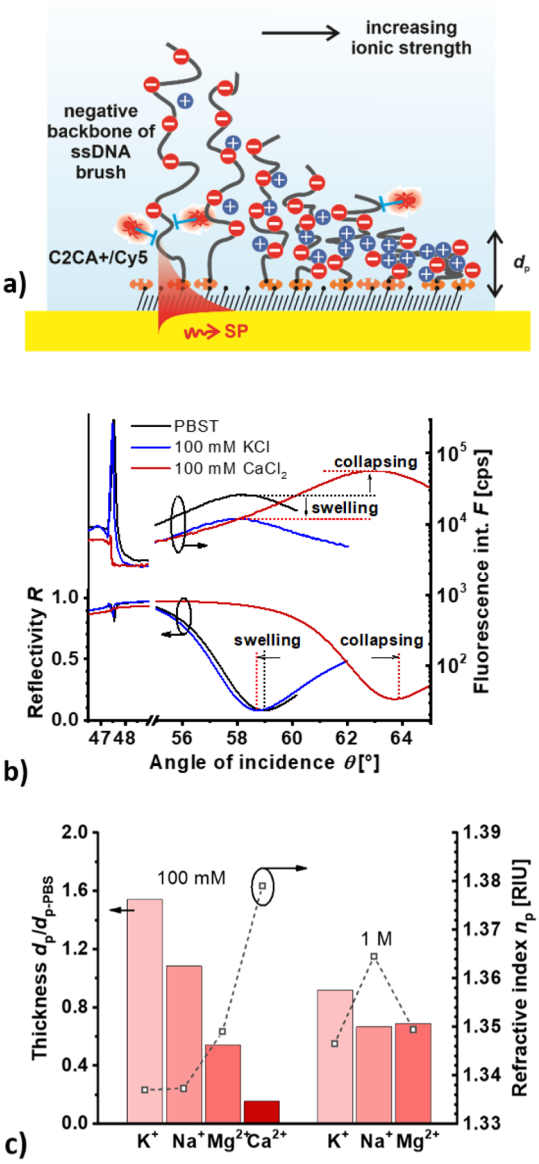

Figure 6. (a) Schematics of the response of the ssDNA brush to different ionic environments. (b) Measured angular reflectivity scans $R(\theta)$ and angular fluorescence intensity scans $F(\theta)$ in 150 mM PBST buffer and in 100 mM KCl and $CaCl_2$ solutions. (c) Evaluated thickness and refractive index changes in respect to the 2.2 μm-thick brush in PBST buffer in electrolytes containing monovalent and divalent cations at different concentrations.

enhanced fluorescence intensity. The expansion is seen as a shift of the SPR angle to lower values and a drop in the SP-enhanced fluorescence intensity. The analysis of the reflectivity curves $R(\theta)$ revealed that the ssDNA brush expanded, and its thickness d_p increased by a factor of 2.2 and 1.1 (compared to that measured in PBST $d_{p\text{-}PBST}$) when the surface-bound ssDNA strands were exposed to a solution with K^+ and Na^+ ions, respectively, at a molar concentration of 100 mM. Interestingly, the divalent Mg^{2+} and Ca^{2+} ions impose an opposite effect, and a decrease in the thickness d_p by a factor of 1.6 and 6.6 is observed, respectively, at the same 100 mM concentration. The particularly strong collapse of the brush in the presence of Ca^{2+} suggests a specific effect of this ion as all other compounds, K^+, Na^+, and Mg^{2+}, did not produce a

https://doi.org/10.1021/acsami.1c03715
ACS Appl. Mater. Interfaces XXXX, XXX, XXX−XXX

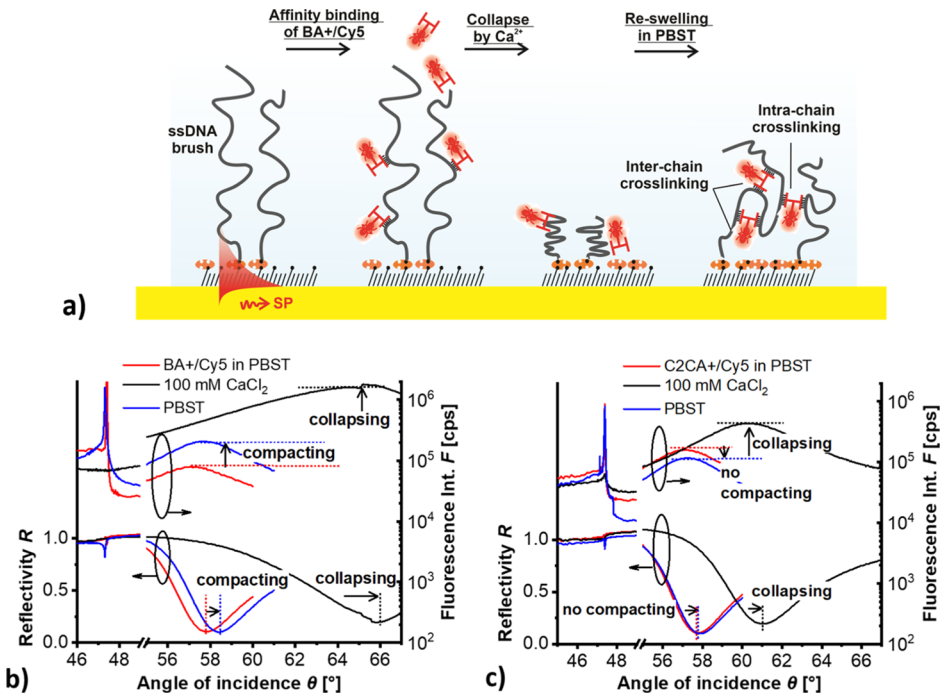

Figure 7. (a) Schematics of the affinity binding of BA staples to the ssDNA brush and its compression by incubation with $CaCl_2$ and re-swelling. Measured angular reflectivity scans $R(\theta)$ and angular fluorescence intensity scans $F(\theta)$ for (b) for the incubation in 100 mM $CaCl_2$ followed by rinsing with PBST and (c) for control experiment with the RCA brush that was affinity reacted with C2CA+/Cy5.

similarly strong change even at 1 M concentration; see Figure 6c. In PBST, the peak fluorescence intensity upon the probing by SPs was $F_{SP(PBST)} = 2.6 \times 10^4$ cps, whereas for the excitation via the OW mode, it was 1 order of magnitude stronger, $F_{TM1(PBST)} = 3.9 \times 10^5$ cps. This difference can be attributed to the fact that the volume probed by the OW mode is larger and thus enables excitation of all Cy5 fluorophores inside the brush. In the presence of monovalent K^+ ions at a concentration of 100 mM, the fluorescence intensity of the fluorescence peak accompanied with the SP mode excitation decreased by a factor of 2.1, which indicates that the ssDNA strands stretched away from the sensor surface, and therefore, fewer fluorophores could be excited by its confined field. In the presence of Ca^{2+} ions at a concentration of 100 mM, the fluorescence intensity excited via SPs in close vicinity of the metal surface increased by a factor of 2.2. These changes confirm the observations obtained from the fitting of reflectivity curves, and the difference in the magnitude of the decrease and increase factors can be attributed to the additional effect of bleaching.

Let us note that similar observations have been attributed to the negatively charged ssDNA backbone that changes its molecular conformation and gets compacted through electrostatic crosslinking in buffers containing Ca^{2+} and Mg^{2+}.[23,57] Our results revealed a much stronger impact of Ca^{2+} ions that can be ascribed to this effect, while Mg^{2+} ions mainly seem to contribute to the Debye screening of the charge interactions, probably due to the higher affinity of Ca^{2+} ions to the DNA bases.[58] Importantly, the changes generated by the exposure of the ssDNA brush to Ca^{2+}, Mg^{2+}, K^+, and Na^+ are reversible, and the ssDNA brush re-arranged its structure back to the original state after rinsing with PBST.

An additional route to manipulate the long ssDNA chains is explored based on short oligonucleotides that carry two sequences complementary to spatially separated parts of ssDNA repeating motifs generated by RCA. Such oligonucleotides can serve as staples that crosslink the neighboring polymer chains or force the individual chains to fold and take on a more compact conformation. As seen in Figure 7a, this approach was investigated using a nucleotide, BA+/Cy5, which has two binding parts with complementary sequences to the RCA-generated ssDNA chains (marked in the sequences presented in Table 1). After flowing the 10 nM solution with BA+/Cy5 over the surface with the ssDNA brush for 15 min, the molecules diffuse inside the polymer architecture and bind (as seen from the comparison of the angular fluorescence scans $F(\theta)$ in Figure S1). The binding occurs in the whole volume of the brush architecture as the fluorescence signal increased in both SP-enhanced fluorescence (peak at $\theta = 58.5°$, probing the volume close to the chip surface) and OW-enhanced fluorescence (peak close to the critical angle exciting the fluorescence throughout the brush).

Interestingly, the binding of BA+/Cy5 did not significantly change the conformation of the ssDNA chains, as the angular positions of SP and OW modes were not altered. This indicates that the BA+ sequences were predominantly able to bind with one of its parts and did not act as crosslinks. Therefore, the ssDNA chains hybridized with BA+/Cy5 staples were exposed to 100 mM Ca^{2+}, which was shown to compact the ssDNA chains and enable bringing their spatially distinct segments closer to each other. As can be seen in Figure 7b, the Ca^{2+} ions induced a strong shift of the SP resonant angle to about $\theta = 66°$ on the brush reacted with BA+/Cy5, which corresponds to a collapse by a factor of 65, as obtained from fitting the reflectivity curves $R(\theta)$. This value is stronger than the factor of 26 observed for the same brush hybridized with C2CA+/Cy5 (Figure 7c), and it can be ascribed to the additional effect of BA+/5 crosslinking of ssDNA chains. In addition, the collapse leads to a more pronounced change than that observed in Figure 6b,c (which is assumed to be caused by

https://doi.org/10.1021/acsami.1c03715
ACS Appl. Mater. Interfaces XXXX, XXX, XXX−XXX

diluting the surface density of ssDNA chains tethered on the surface with $\sigma = 3.2 \times 10^{-6}$ nmol/mm^2). Moreover, when switching back to PBST, the ssDNA brush hybridized with the C2CA+ sequence returned to its original state, but the one modified with BA+/Cy5 partially retained the collapsed nature, as documented by the shifted SPR angle and increased SP-enhanced fluorescence peak. The intensity of the SP-enhanced fluorescence signal increased in PBST by a factor of 2.7 after the collapse of the BA+/Cy5 structure, while that of C2CA5+/Cy5 decreased by a factor of 1.33. These changes are in agreement with those obtained from fitting $R(\theta)$ and confirm that the stronger compression of the ssDNA brush architecture can be obtained by a combination of crosslinking with specific DNA staples and ionic environment change.

CONCLUSIONS

For the first time, we report on the *in situ* and real-time observation of RCA prolongation of ssDNA chains above 10 μm when attached to a solid surface. The grown ssDNA chains take the form of a brush, and they are probed by a combination of SPR and OWS methods, enabled by the fact that a sufficiently thick polymer layer can serve as an optical dielectric waveguide. The analysis of the spectrum of guided waves traveling along this interface with "grafted-from" densely packed ssDNA chains provides an efficient means to monitor their elongation and determine key characteristics of the RCA reaction on a solid surface. Such observations are difficult to achieve with other techniques that are typically only able to characterize the DNA brush after its synthesis is finished, and their use is complicated by the soft and fragile nature of the ssDNA brush. On the other hand, it is worth noting that the presented approach provides detailed information only when the thickness of the brush layer is sufficiently high (several micrometers) and the probing of the interface over an area of about one mm^2 is needed in order to record sharp dielectric OW resonances. Due to this fact, it is not feasible to investigate the behavior of sparsely immobilized DNA chains that do not form the thick brush layers when small amounts of padlock probes are immobilized on the solid surface. We demonstrate how this platform can be used to monitor conformation changes of ssDNA in response to an ionic strength-triggered collapse of the ssDNA brush and its intra- and inter-chain crosslinking via specifically designed oligonucleotide staples. A combination of DNA staples and ionic change allowed compacting the RCA-generated brush by a factor of >10, which can be useful in analytical application with plasmonic biosensor readout for enhancing the sensitivity by dragging the molecules to the plasmonic hotspot on the surface.

ASSOCIATED CONTENT

Supporting Information

The Supporting Information is available free of charge at https://pubs.acs.org/doi/10.1021/acsami.1c03715.

Details on the operation of the used optical configuration, used mathematical model for the analysis of the thin ssDNA brush layer, and example optical spectra for the probing of the thin ssDNA brush layer by combined SPR, OWS, and SPFS (PDF)

AUTHOR INFORMATION

Corresponding Author

Jakub Dostalek − *Biosensor Technologies, AIT-Austrian Institute of Technology GmbH, 3430 Tulln an der Donau, Austria; FZU-Institute of Physics, Czech Academy of Sciences, Prague 182 21, Czech Republic;* orcid.org/0000-0002-0431-2170; Phone: +43 (0) 6642351773; Email: jakub.dostalek@ait.ac.at; Fax: +43 (0) 505504450

Authors

Bernadette Lechner − *Biosensor Technologies, AIT-Austrian Institute of Technology GmbH, 3430 Tulln an der Donau, Austria; CEST Competence Center for Electrochemical Surface Technologies, 3430 Tulln an der Donau, Austria;* orcid.org/0000-0002-4949-5118

Simone Hageneder − *Biosensor Technologies, AIT-Austrian Institute of Technology GmbH, 3430 Tulln an der Donau, Austria;* orcid.org/0000-0002-7200-3257

Katharina Schmidt − *Biosensor Technologies, AIT-Austrian Institute of Technology GmbH, 3430 Tulln an der Donau, Austria*

Mark P. Kreuzer − *Biosensor Technologies, AIT-Austrian Institute of Technology GmbH, 3430 Tulln an der Donau, Austria; Instituto de Nanosistemas, Universidad Nacional de San Martín, San Martín CP 1650 Provincia de Buenos Aires, Argentina*

Rick Conzemius − *Molecular Diagnostics, Health & Environment, AIT Austrian Institute of Technology GmbH, 1210 Vienna, Austria*

Erik Reimhult − *Institute for Biologically Inspired Materials, Department of Nanobiotechnology, University of Natural Resources and Life Sciences Vienna (BOKU), Vienna 1190, Austria;* orcid.org/0000-0003-1417-5576

Ivan Barišić − *Molecular Diagnostics, Health & Environment, AIT Austrian Institute of Technology GmbH, 1210 Vienna, Austria;* orcid.org/0000-0002-1301-6197

Complete contact information is available at: https://pubs.acs.org/10.1021/acsami.1c03715

Author Contributions

S.H. and B.L. contributed equally. All authors have given approval to the final version of the manuscript.

Notes

The authors declare no competing financial interest.

ACKNOWLEDGMENTS

This work was supported by the Austrian Research Promotion Agency (FFG) with ERANET project PLABAN, grant agreement no. 861578, and by the program FemTech. In addition, J.D. acknowledges support from the ESIF and MEYS (FZU researchers, technical and administrative staff mobility—CZ.02.2.69/0.0/0.0/18_053/0016627). M.P.K acknowledges the funding from European Commission via H2020 Marie Skłodowska-Curie Actions project HYMADE with grant agreement no. 645686.

REFERENCES

(1) Boehm, C. D. Use of Polymerase Chain Reaction for Diagnosis of Inherited Disorders. *Clin. Chem.* **1989**, *35*, 1843−1848.

(2) Lynch, C.; Fleming, R. A Review of Direct Polymerase Chain Reaction of DNA and RNA for Forensic Purposes. *Wiley Interdiscip. Rev.: Comput. Mol. Sci.* **2019**, *1*, No. e1335.

(3) Cree, I. A. Diagnostic RAS Mutation Analysis by Polymerase Chain Reaction (PCR). *Biomol. Detect. Quantif.* **2016**, *8*, 29−32.
(4) Yang, S.; Rothman, R. E. PCR-Based Diagnostics for Infectious Diseases: Uses, Limitations, and Future Applications in Acute-Care Settings. *Lancet Infect. Dis.* **2004**, *4*, 337−348.
(5) De Medici, D.; Kuchta, T.; Knutsson, R.; Angelov, A.; Auricchio, B.; Barbanera, M.; Diaz-Amigo, C.; Fiore, A.; Kudirkiene, E.; Hohl, A.; Horvatek Tomic, D.; Gotcheva, V.; Popping, B.; Prukner-Radovcic, E.; Scaramaglia, S.; Siekel, P.; To, K. A.; Wagner, M. Rapid Methods for Quality Assurance of Foods: The Next Decade with Polymerase Chain Reaction (PCR)-Based Food Monitoring. *Food Anal. Methods* **2015**, *8*, 255−271.
(6) Dewey, F. E.; Pan, S.; Wheeler, M. T.; Quake, S. R.; Ashley, E. A. DNA Sequencing Clinical Applications of New DNA Sequencing Technologies. *Circulation* **2012**, *125*, 931−944.
(7) Wood, S. A.; Pochon, X.; Laroche, O.; Ammon, U.; Adamson, J.; Zaiko, A. A Comparison of Droplet Digital Polymerase Chain Reaction (PCR), Quantitative PCR and Metabarcoding for Species-Specific Detection in Environmental DNA. *Mol. Ecol. Resour.* **2019**, *19*, 1407−1419.
(8) Wittwer, C. T.; Herrmann, M. G.; Gundry, C. N.; Elenitoba-Johnson, K. S. J. Real-Time Multiplex PCR Assays. *Methods* **2001**, *25*, 430−442.
(9) Liu, D.; Daubendiek, S. L.; Zillman, M. A.; Ryan, K.; Kool, E. T. Rolling Circle DNA Synthesis: Small Circular Oligonucleotides as Efficient Templates for DNA Polymerases. *J. Am. Chem. Soc.* **1996**, *118*, 1587−1594.
(10) Fire, A.; Xu, S. Q. Rolling Replication of Short DNA Circles. *Proc. Natl. Acad. Sci. U.S.A.* **1995**, *92*, 4641−4645.
(11) Zanoli, L.; Spoto, G. Isothermal Amplification Methods for the Detection of Nucleic Acids in Microfluidic Devices. *Biosensors* **2013**, *3*, 18−43.
(12) Lau, H. Y.; Botella, J. R. Advanced DNA-Based Point-of-Care Diagnostic Methods for Plant Diseases Detection. *Front. Plant Sci.* **2017**, *8*, 1−14.
(13) Notomi, T.; Okayama, H.; Masubuchi, H.; Yonekawa, T.; Watanabe, K.; Amino, N.; Hase, T. Loop-Mediated Isothermal Amplification of DNA. *Nucleic Acids Res.* **2000**, *28*, No. e63.
(14) Lizardi, P. M.; Huang, X.; Zhu, Z.; Bray-Ward, P.; Thomas, D. C.; Ward, D. C. Mutation Detection and Single-Molecule Counting Using Isothermal Rolling-Circle Amplification. *Nat. Genet.* **1998**, *19*, 225−232.
(15) Barišić, I.; Petzka, J.; Schoenthaler, S.; Vierlinger, K.; Noehammer, C.; Wiesinger-Mayr, H. Multiplex Characterization of Human Pathogens Including Species and Antibiotic-Resistance Gene Identification. *J. Med. Microbiol.* **2016**, *65*, 48−55.
(16) Adessi, C. Solid Phase DNA Amplification: Characterisation of Primer Attachment and Amplification Mechanisms. *Nucleic Acids Res.* **2000**, *28*, No. e87.
(17) Tjong, V.; Yu, H.; Hucknall, A.; Rangarajan, S.; Chilkoti, A. Amplified On-Chip Fluorescence Detection of DNA Hybridization by Surface-Initiated Enzymatic Polymerization. *Anal. Chem.* **2011**, *83*, 5153−5159.
(18) Ericsson, O.; Jarvius, J.; Schallmeiner, E.; Howell, M.; Nong, R. Y.; Reuter, H.; Hahn, M.; Stenberg, J.; Nilsson, M.; Landegren, U. A Dual-Tag Microarray Platform for High-Performance Nucleic Acid and Protein Analyses. *Nucleic Acids Res.* **2008**, *36*, No. e45.
(19) Chi, Y. S.; Jung, Y. H.; Choi, I. S.; Kim, Y.-G. Surface-Initiated Growth of Poly d(A-T) by Tag DNA Polymerase. *Langmuir* **2005**, *21*, 4669−4673.
(20) Chow, D. C.; Chilkoti, A. Surface-Initiated Enzymatic Polymerization of DNA. *Langmuir* **2007**, *23*, 11712−11717.
(21) Bracha, D.; Karzbrun, E.; Daube, S. S.; Bar-Ziv, R. H. Emergent Properties of Dense DNA Phases toward Artificial Biosystems on a Surface. *Acc. Chem. Res.* **2014**, *47*, 1912−1921.
(22) Huang, F.; Zhou, X.; Yao, D.; Xiao, S.; Liang, H. DNA Polymer Brush Patterning through Photocontrollable Surface-Initiated DNA Hybridization Chain Reaction. *Small* **2015**, *11*, 5800−5806.
(23) Petrovykh, D. Y.; Kimura-Suda, H.; Whitman, L. J.; Tarlov, M. J. Quantitative Analysis and Characterization of DNA Immobilized on Gold. *J. Am. Chem. Soc.* **2003**, *125*, 5219−5226.
(24) Khan, M. N.; Tjong, V.; Chilkoti, A.; Zharnikov, M. Spectroscopic Study of a DNA Brush Synthesized in Situ by Surface Initiated Enzymatic Polymerization. *J. Phys. Chem. B* **2013**, *117*, 9929−9938.
(25) Barbee, K. D.; Chandrangsu, M.; Huang, X. Fabrication of DNA Polymer Brush Arrays by Destructive Micropatterning and Rolling-Circle Amplification. *Macromol. Biosci.* **2011**, *11*, 607−617.
(26) Palanisamy, R.; Connolly, A. R.; Trau, M. Considerations of Solid-Phase DNA Amplification. *Bioconjugate Chem.* **2010**, *21*, 690−695.
(27) Dostálek, J.; Knoll, W. Plasmonics. In *Polymer Science: A Comprehensive Reference*; Matyjaszewski, K., Möller, M., Eds.; Elsevier B.V.: Amsterdam, 2012; Vol. 2, pp 647−659.
(28) Homola, J. Surface Plasmon Resonance Sensors for Detection of Chemical and Biological Species. *Chem. Rev.* **2008**, *108*, 462−493.
(29) Beines, P. W.; Klosterkamp, I.; Menges, B.; Jonas, U.; Knoll, W. Responsive Thin Hydrogel Layers from Photo-Cross-Linkable Poly(N-Isopropylacrylamide) Terpolymers. *Langmuir* **2007**, *23*, 2231−2238.
(30) Toomey, R.; Freidank, D.; Rühe, J. Swelling Behavior of Thin, Surface-Attached Polymer Networks. *Macromolecules* **2004**, *37*, 882−887.
(31) Ferrand-Drake Del Castillo, G.; Emilsson, G.; Dahlin, A. Quantitative Analysis of Thickness and PH Actuation of Weak Polyelectrolyte Brushes. *J. Phys. Chem. C* **2018**, *122*, 27516−27527.
(32) Zhang, Q.; Wang, Y.; Mateescu, A.; Sergelen, K.; Kibrom, A.; Jonas, U.; Wei, T.; Dostalek, J. Biosensor Based on Hydrogel Optical Waveguide Spectroscopy for the Detection of 17β-Estradiol. *Talanta* **2013**, *104*, 149−154.
(33) Junk, M. J. N.; Anac, I.; Menges, B.; Jonas, U. Analysis of Optical Gradient Profiles during Temperature- and Salt-Dependent Swelling of Thin Responsive Hydrogel Films. *Langmuir* **2010**, *26*, 12253−12259.
(34) Toma, M.; Jonas, U.; Mateescu, A.; Knoll, W.; Dostalek, J. Active Control of SPR by Thermoresponsive Hydrogels for Biosensor Applications. *J. Phys. Chem. C* **2013**, *117*, 11705−11712.
(35) Wang, Y.; Brunsen, A.; Jonas, U.; Dostálek, J.; Knoll, W. Prostate Specific Antigen Biosensor Based on Long Range Surface Plasmon-Enhanced Fluorescence Spectroscopy and Dextran Hydrogel Binding Matrix. *Anal. Chem.* **2009**, *81*, 9625−9632.
(36) Stengel, G.; Knoll, W. Surface Plasmon Field-Enhanced Fluorescence Spectroscopy Studies of Primer Extension Reactions. *Nucleic Acids Res.* **2005**, *33*, No. e69.
(37) Tumolo, T.; Angnes, L.; Baptista, M. S. Determination of the Refractive Index Increment (Dn/Dc) of Molecule and Macromolecule Solutions by Surface Plasmon Resonance. *Anal. Biochem.* **2004**, *333*, 273−279.
(38) Theisen, A.; Johann, C.; Deacon, M. P.; Harding, S. *Refractive Increment Data-Book for Polymer and Biomolecular Scientists*; Nottingham University Press: Nottingham, 2000.
(39) Nilsson, M.; Malmgren, H.; Samiotaki, M.; Kwiatkowski, M.; Chowdhary, B.; Landegren, U. Padlock Probes: Circularizing Oligonucleotides for Localized DNA Detection. *Science* **1994**, *265*, 2085−2088.
(40) Barišić, I.; Schoenthaler, S.; Ke, R.; Nilsson, M.; Noehammer, C.; Wiesinger-Mayr, H. Multiplex Detection of Antibiotic Resistance Genes Using Padlock Probes. *Diagn. Microbiol. Infect. Dis.* **2013**, *77*, 118−125.
(41) Su, X.; Wu, Y.-J.; Robelek, R.; Knoll, W. Surface Plasmon Resonance Spectroscopy and Quartz Crystal Microbalance Study of Streptavidin Film Structure Effects on Biotinylated DNA Assembly and Target DNA Hybridization. *Langmuir* **2005**, *21*, 348−353.
(42) Tsortos, A.; Papadakis, G.; Mitsakakis, K.; Melzak, K. A.; Gizeli, E. Quantitative Determination of Size and Shape of Surface-Bound DNA Using an Acoustic Wave Sensor. *Biophys. J.* **2008**, *94*, 2706−2715.

https://doi.org/10.1021/acsami.1c03715
ACS Appl. Mater. Interfaces XXXX, XXX, XXX−XXX

(43) Thibault, T.; Degrouard, J.; Baril, P.; Pichon, C.; Midoux, P.; Malinge, J.-M. Production of DNA Minicircles Less than 250 Base Pairs through a Novel Concentrated DNA Circularization Assay Enabling Minicircle Design with NF-KB Inhibition Activity. *Nucleic Acids Res.* **2017**, *45*, No. e26.
(44) He, P.; Liu, L.; Qiao, W.; Zhang, S. Ultrasensitive Detection of Thrombin Using Surface Plasmon Resonance and Quartz Crystal Microbalance Sensors by Aptamer-Based Rolling Circle Amplification and Nanoparticle Signal Enhancement. *Chem. Commun.* **2014**, *50*, 1481−1484.
(45) Huang, Y.-Y.; Hsu, H.-Y.; Huang, C.-J. C. A Protein Detection Technique by Using Surface Plasmon Resonance (SPR) with Rolling Circle Amplification (RCA) and Nanogold-Modified Tags. *Biosens. Bioelectron.* **2007**, *22*, 980−985.
(46) Shi, D.; Huang, J.; Chuai, Z.; Chen, D.; Zhu, X.; Wang, H.; Peng, J.; Wu, H.; Huang, Q.; Fu, W. Isothermal and Rapid Detection of Pathogenic Microorganisms Using a Nano-Rolling Circle Amplification-Surface Plasmon Resonance Biosensor. *Biosens. Bioelectron.* **2014**, *62*, 280−287.
(47) Xiang, Y.; Deng, K.; Xia, H.; Yao, C.; Chen, Q.; Zhang, L.; Liu, Z.; Fu, W. Isothermal Detection of Multiple Point Mutations by a Surface Plasmon Resonance Biosensor with Au Nanoparticles Enhanced Surface-Anchored Rolling Circle Amplification. *Biosens. Bioelectron.* **2013**, *49*, 442−449.
(48) Xiang, Y.; Zhu, X.; Huang, Q.; Zheng, J.; Fu, W. Real-Time Monitoring of Mycobacterium Genomic DNA with Target-Primed Rolling Circle Amplification by a Au Nanoparticle-Embedded SPR Biosensor. *Biosens. Bioelectron.* **2015**, *66*, 512−519.
(49) Soengas, M. S.; Gutiérrez, C.; Salas, M. Helix-Destabilizing Activity of Φ29 Single-Stranded DNA Binding Protein: Effect on the Elongation Rate during Strand Displacement DNA Replication. *J. Mol. Biol.* **1995**, *253*, 517−529.
(50) Gil, P. S.; Lacks, D. J.; Parisse, P.; Casalis, L.; Nkoua Ngavouka, M. D. Single-Stranded DNA Oligomer Brush Structure Is Dominated by Intramolecular Interactions Mediated by the Ion Environment. *Soft Matter* **2018**, *14*, 9675−9680.
(51) Rao, A. N.; Grainger, D. W. Biophysical Properties of Nucleic Acids at Surfaces Relevant to Microarray Performance. *Biomater. Sci.* **2014**, *2*, 436−471.
(52) Nkoua Ngavouka, M. D.; Bosco, A.; Casalis, L.; Parisse, P. Determination of Average Internucleotide Distance in Variable Density SsDNA Nanobrushes in the Presence of Different Cations Species. *Macromolecules* **2014**, *47*, 8748−8753.
(53) Castelino, K.; Kannan, B.; Majumdar, A. Characterization of Grafting Density and Binding Efficiency of DNA and Proteins on Gold Surfaces. *Langmuir* **2005**, *21*, 1956−1961.
(54) Herne, T. M.; Tarlov, M. J. Characterization of DNA Probes Immobilized on Gold Surfaces. *J. Am. Chem. Soc.* **1997**, *119*, 8916−8920.
(55) Gong, P.; Levicky, R. DNA Surface Hybridization Regimes. *Proc. Natl. Acad. Sci. U.S.A.* **2008**, *105*, 5301−5306.
(56) Peterson, A. W. The Effect of Surface Probe Density on DNA Hybridization. *Nucleic Acids Res.* **2001**, *29*, 5163−5168.
(57) Bosco, A.; Camunas-Soler, J.; Ritort, F. Elastic Properties and Secondary Structure Formation of Single-Stranded DNA at Monovalent and Divalent Salt Conditions. *Nucleic Acids Res.* **2014**, *42*, 2064−2074.
(58) Hackl, E. V.; Kornilova, S. V.; Blagoi, Y. P. DNA Structural Transitions Induced by Divalent Metal Ions in Aqueous Solutions. *Int. J. Biol. Macromol.* **2005**, *35*, 175−191.

https://doi.org/10.1021/acsami.1c03715
ACS Appl. Mater. Interfaces XXXX, XXX, XXX−XXX